Evaluation of IEM, Dubois, and Oh Radar Backscatter Models Using Airborne L-Band SAR

Rocco Panciera, *Member, IEEE*, Mihai A. Tanase, *Member, IEEE*, Kim Lowell, and Jeffrey P. Walker, *Member, IEEE*

***Abstract*—The backscatter predicted by three common surface scattering models (the Integral Equation Model (IEM), the Dubois, and the Oh models) was evaluated against fully polarized L-band airborne observations. Before any site-specific calibration, the Oh model was found to be the most accurate among the three, with mean errors between the simulated and the observed backscatter of 1.2 dB (±2.6 dB standard deviation of the error) and −0.4 dB (±2.4 dB) for HH and VV polarizations, respectively, while the IEM and Dubois presented larger errors, with a maximum of 4.5 dB (±2 dB) for the IEM in VV polarization. The backscatter errors were observed to be related to surface roughness, another major factor determining the electromagnetic scattering at the soil surface. An existing semiempirical calibration of the surface roughness correlation length was therefore applied to improve the mismatch between modeled and observed backscatters. The application of the semiempirical calibration led to a significant improvement of the backscatter prediction for the IEM. After calibration, the IEM outperformed the Oh model, resulting in a mean backscatter error of −0.3 dB (±1.1 dB) and −0.2 (±1.2 dB) for HH and VV polarizations, respectively. To test the robustness of the semiempirical calibration, calibration functions derived from an independent data set were applied and shown to also improve the (uncalibrated) IEM performance, suggesting that the calibration procedure is relatively robust for global application.**

***Index Terms*—Airborne radar, scattering, soil, synthetic aperture radar (SAR).**

I. Introduction

SYNTHETIC aperture radar (SAR) is a promising option for the temporal monitoring of near-surface soil moisture at a spatial and temporal resolution suitable for hydrological and agricultural applications. The extraction of accurate soil moisture information from SAR data is subject to the accurate modeling of the relative contribution of soil moisture and surface roughness to the power backscattered at the soil surface. Among the numerous surface scattering models reported in the literature, the most widely applied are a physical model, the Integral Equation Model (IEM) developed in [1], and two semiempirical models, the Dubois [2] and the Oh [3] models. Semiempirical models provide relatively simple relationships between surface properties and SAR metrics that reflect to a certain extent the physics of the scattering mechanisms. However, they rely on parameters that are often site specific and therefore valid only for specific soil conditions. Conversely, physical approaches are based on electromagnetic scattering theory and, even though they provide site-independent relationships, are mathematically more complex and involve a heavier computational burden.

Each of the models has been extensively tested in laboratory conditions and tower-mounted sensors [2], [4]–[7]. However, the testing of such models using airborne or spaceborne SAR over natural and agricultural surfaces has been mainly focused on the previous generation of C-band SAR sensors such as RADARSAT and European Remote-Sensing Satellite (ERS) [8]–[12]. Only a few studies have assessed the models individually using L-band data [13]–[16], and a direct intercomparison of all three models with L-band multipolarized data is currently lacking. Previous studies provided contrasting results on the accuracy of the individual models at L-band, with most reporting discrepancies between the modeled and observed backscatters which can render soil moisture estimation using such models inaccurate. Only one study reported an unbiased agreement between IEM-simulated and observed backscatters at both polarizations [15]. Other studies have indicated a tendency of the IEM to overestimate the L-band observed backscatters, by up to 3–5 dB for rough surfaces (surface root mean square (rms) > 1 cm) [13]. Nevertheless, the IEM and the Dubois model were generally found to be more accurate than earlier versions [6], [17] of the Oh model [14], [16]. Generally, the uncertainty on surface roughness (including measurement error, multiscale effects, and spatial heterogeneity) has been addressed as a major factor in the failure of the models to reproduce the backscatters observed by airborne and spaceborne sensors [9], [13], [18].

The characterization of surface roughness has been traditionally based on three parameters, namely, the rms of the surface heights (hereby referred to as "surface rms"), the correlation length, and the shape of the autocorrelation function (ACF) [18]. The empirical ACF is usually approximated using an exponential or Gaussian function. However, measuring the correlation length is a problematic task. Due the large spatial variability and multiscale nature of natural and agricultural surfaces [19], surface roughness parameters estimated from field measurements are very sensitive to the length of the profile over which they are measured [20]. In order to overcome this problem, a few studies have proposed semiempirical calibrations of the surface roughness correlation length [8], [9],

Manuscript received May 22, 2013; revised August 19, 2013; accepted September 22, 2013. This work was supported by an Australian Research Council Super Science Fellowship (FS100100040). The Soil Moisture Active passive Experiments (SMAPEx) experiments were funded by an Australian Research Council Discovery Project (DP0984586).

R. Panciera, M. A. Tanase, and K. Lowell are with the Cooperative Research Centre for Spatial Information, The University of Melbourne, Melbourne, Vic. 3053, Australia (e-mail: panr@unimelb.edu.au).

J. P. Walker is with the Department of Civil Engineering, Monash University, Melbourne, Vic. 3800, Australia.

Digital Object Identifier 10.1109/TGRS.2013.2286203

0196-2892 © 2013 IEEE. Personal use is permitted, but republication/redistribution requires IEEE permission.
See http://www.ieee.org/publications_standards/publications/rights/index.html for more information.

[12], [21]–[23], the most difficult surface parameter to measure and characterize spatially, with considerable improvement in the performance of the model reported after semiempirical calibration. The methodology proposed in those studies consists of replacing the measured correlation length by a semiempirical fitting parameter ("Lopt") which aims at compensating for measurement and model errors associated to the roughness correlation length. The fitting parameter was found to be linked to the surface roughness, increasing with increasing surface rms by either a linear, exponential, or power calibration function, with the exact relationship $\mathrm{Lopt} = \mathrm{f}$ (rms) being dependent on the sensor incidence angle, polarization, and frequency [9]. For a fixed surface rms, Lopt was reported to decrease strongly with increasing incidence angle at both C-band [22] and X-band [23]. The variation of Lopt with sensor frequency changed depending upon the assumption made in the IEM regarding the shape of the surface ACF, resulting in either a decrease (for Gaussian ACF) or increase (for exponential ACF) of Lopt with frequency increasing from L-band to X-band [22], [23]. Once appropriate equations for the fitting parameter Lopt are defined for a given sensor configuration, Lopt can be calculated for the known surface rms. The advantage of the procedure is that the number of surface parameters needed to characterize the backscatter is reduced from three (soil moisture, surface rms, and correlation length) to two (soil moisture and surface rms). Equations for the fitting parameter Lopt have been reported to date for C-band [8], [9], [12], [22], and X-band [23]. However, to date, limited attention has been devoted to estimating the fitting parameter for L-band data; values for the fitting parameter Lopt were provided in [9] for L-band observations at HH polarization and a limited range of incidence angles (44°–57°), but no function was fitted. Alternative approaches have been proposed that calibrate both the surface rms and correlation length using linear regression functions dependent on the backscatter itself [24]. However, in this study, the approach in [8], [9], [12], [22], and [23] is preferred as it provides a set of functional relationships between the fitting parameters and the surface rms as a function incidence angle, polarization, and frequency, rather than a site-specific regression between effective roughness parameters and the SAR backscatter as in [24].

The objective of this paper is to compare the accuracy of the backscatter simulated by the IEM, Dubois, and Oh models for the first time using fully polarized airborne L-band observations and to assess the potential improvement of the model performance at L-band through the semiempirical calibration of the surface roughness parameters. To that end, first, the impact of using roughness parameters associated with both the soil clods and tillage structure scales is analyzed to select the most suitable roughness parameters. The performances of the three models are then compared "as is," i.e., without applying any calibration. Possible causes of the mismatch between the observed and the simulated backscatter are then assessed and discussed. The semiempirical calibration proposed in [8], [9], [12], [22], and [23] is then applied to the models exhibiting the best performance (IEM and Oh), and the robustness of the calibration procedures is assessed and discussed.

II. Study Area and Data Sets

The airborne and ground data used in this study were collected during the Third Soil Moisture Active Passive Experiment (SMAPEx-3), conducted from September 5 to 23, 2011, in the Yanco study area in southeastern Australia [25]. The site is a semiarid agricultural and grazing area located in the western plains of the Murrumbidgee catchment near the township of Yanco (longitude $146°10'$E, latitude $34°50'$S). The topography of the study area is flat with elevation ranging from 117 to 150 m. Approximately one-third of the area is characterized by intense irrigation activity. The principal summer crops grown are rice, corn, and soybeans, while winter crops include wheat, barley, oats, and canola. Moderate rainfall in the first half of the experiment was followed by a dry-down period that resulted in dry to intermediate soil moisture conditions (0–0.2 $\mathrm{m}^3/\mathrm{m}^3$), although for many irrigated fields, higher values (up to 0.4 $\mathrm{m}^3/\mathrm{m}^3$) were measured.

Surface backscatter measurements were acquired by the polarimetric L-band imaging SAR (PLIS) [26] on nine dates (September 5th, 7th, 10th, 13th, 15th, 18th, 19th, 21st, and 23rd), with coincident ground sampling of soil moisture. PLIS is a fully polarimetric L-band (1.26 GHz) SAR sensor which illuminates the ground on either sides of the aircraft at an incidence angle varying from 15° to 45° across the swath. Using a 30-MHz bandwidth, the single-look resolution is approximately 6 m (slant range) and 0.8 m (azimuth), which resulted in a ground-projected range resolution between 12 m (near range) and 8 m (far range). The PLIS mean ground swath is 2200 m on both sides of the aircraft from an altitude of 3000 m. PLIS polarimetric calibration was accomplished using a modified version of the distributed target method described in [27], using a distributed forest target in conjunction with six trihedral passive radar calibrators (PRCs). The polarimetrically calibrated data exhibited a mean ratio of the copolarized channels of 1 and mean phase differences of 3° and 6° for the left and the right antenna, respectively. After radiometric calibration, the mean difference between the radar cross section observed over the six PRCs and the theoretical one was 0.9 dB. This was calculated as the mean of the differences for all days and two daily calibration runs undertaken before and after scientific flights (absolute calibration accuracy). Such differences changed from day to day and even changed sign between pre- and postscientific flight calibration runs, making it unfeasible to further correct for such offsets even if only on a daily basis. The standard deviation of all offsets (relative calibration accuracy) was 0.8 dB.

Extensive ground sampling of near-surface (0–5 cm) soil moisture and surface roughness was conducted on rotation at approximately 80 agricultural fields, including several fields presenting bare surface conditions in preparation for the summer crops. Eleven such fields were selected for the purpose of this study. Although surface roughness was measured at 13 bare fields, two fields were excluded from the analysis as they either presented regular banks or were imaged at very steep angles which resulted in an elevated coherent backscatter component (approximately 9 dB higher than bare fields with similar surface roughness but without regular banks).

TABLE I
CHARACTERISTICS OF THE BARE AGRICULTURAL FIELDS AND SUMMARY OF THE GROUND DATA COLLECTED. FOR FIELDS WITH PERIODIC STRUCTURE, THE ROW AZIMUTH ANGLE IS GIVEN. SUPERSCRIPTS IN THE "FIELD #" COLUMN INDICATE FIELDS WITHOUT (∗) AND WITH (+) ACTIVITY OF FARMING MACHINERY RECORDED DURING THE OBSERVATION PERIOD. THE SURFACE ROUGHNESS PARAMETERS INDICATED ARE THE SURFACE HEIGHT ROOT MEAN SQUARE (rms) AND CORRELATION LENGTH (L)

Field #	SAR Inc. Angle	Row Azimuth Angle	Soil Moisture min-max [m^3/m^3]	Surface Roughness [cm] *Fine-scale (along rows)*		*Coarse-scale (across rows)*	
				rms	*L*	*rms*	*L*
87^*	35°	-	0.12-0.18	3.7	9.1	3.7	9.1
48^*	38°	-	0.09-0.12	3.3	15.5	3.3	15.5
49^*	35°	-	0.08-0.10	4.6	20.8	4.6	20.8
50^*	30°	-	0.07-0.16	2.1	9.3	2.1	9.3
14^*	38°	10°	0.05-0.09	2.3	7.2	6.0	18.9
79^*	31°	10°	0.05-0.13	1.0	6.9	1.3	10.6
24^*	38°	140°	0.25-0.27	3.3	11.0	5.1	30.8
1^+	36°	80°	0.14-0.19	2.3	8.0	6.4	23.0
43^+	24°	20°	0.09-0.39	1.1	2.6	6.6	22.3
51^+	24°	110°	0.07-0.38	1.5	10.8	7.6	23.6
70^+	25°	10°	0.12-0.25	1.7	5.7	5.7	22.5

Modeling the backscatter from such fields would require detailed knowledge of the geometry of the regular banks, which was not available. Table I lists the main characteristics of the fields used in this analysis. Soil moisture was monitored at each field on a weekly basis, therefore providing concurrent SAR observation and soil moisture validation data for three dates for each field. Soil moisture measurements were conducted using portable dielectric probes on a regular grid of locations equally spaced at 250 m. At each sampling location, three soil moisture measurements were taken within a 1-m radius and averaged to characterize small scale soil moisture variability. The dielectric probes were Stevens Water Hydraprobe which measure directly the complex soil dielectric constant with a cylindrical volume of soil of 5 cm in length bounded by the probe's three tines. The complex dielectric measurement were then converted to soil moisture (in m^3/m^3) using a calibration approach specifically developed and validated using hundreds of gravimetric samples collected in the study area, yielding an estimated accuracy of 0.035 m^3/m^3 [28].

Surface roughness was measured once during the experiment at each field, using a custom-built surface profiler consisting of a 1-m-long board with 200 pins spaced by 0.5 cm. A minimum of one and up to three measurements were taken within each field to characterize spatial variability in surface roughness. Each roughness measurement consisted of two 3-m-long surface profiles taken in the north–south and east–west directions or, alternatively, in the direction parallel and perpendicular to the crop row directions if these were present. The surface rms and correlation length for each 3-m-long profile were extracted from digital photographs using the digital image processing MATLAB package Quick Profiler (QuiP) [29]. The ground data collected are summarized in Table I. A wide range of surface roughness conditions was analyzed (1–7.6 cm).

On four of the fields analyzed, the activity of farming machinery was recorded during the observation period. This included the mechanical alteration of the soil surface, such as ploughing or tillage. In such cases, the surface roughness parameters, which were measured only once during the experiment, might not be representative of the surface conditions for all the dates considered. This is discussed in more detail in Section V-C. Other than the cases of farming activity, it can be safely assumed that roughness parameters were stable during the observation period, given the absence of significant rainfall events.

III. SURFACE SCATTERING MODELS

Three surface models were considered for this analysis: A theoretical model, the IEM formulated in [1], and two semiempirical models, one developed by Dubois *et al.* [2] and one proposed by Oh [3]. These models are the most widely used for surface scattering simulation and are candidates for use in global soil moisture retrieval (for bare or low vegetated areas) due to their relatively simple structure and ease of inversion and applicability to a wide range of soil moisture, surface roughness, and incidence angles.

The IEM is a theoretical backscattering model applicable to a wide range of roughness conditions. The complete mathematical formulation of the model is too lengthy to be included here but can be found in [1]. The model solves the integral equations for the tangential surface fields, taking into account the incidence angle, the surface rms and ACF (defined for a 1-D roughness profile), and the dielectric constant. A low-frequency approximation of the IEM was used in this study, valid in the region $\mathrm{k} * \mathrm{rms} < 3$ (where k is the wave number $= 2\pi/\lambda$, where λ is the wavelength) in which single scattering terms dominate over multiple scattering terms. Most agricultural surfaces, and all those listed in Table I, fall within this validity domain. The IEM simulations depend heavily on the assumption made concerning the shape (exponential or Gaussian) of the ACF. Several studies have found that, for agricultural surfaces, the exponential function provides the best results [9], [15].

Dubois *et al.* [2] developed a semiempirical approach that expresses the radar backscatter coefficients as a function of incidence angle (θ), dielectric constant (ε_r), surface rms, and wavelength as

$$\sigma^0_{HH} = 10^{-2.75}\left(\frac{\cos^{1.5}\theta}{\sin^5\theta}\right)10^{0.028\varepsilon_r\tan\theta}\lambda^{0.7}(\mathrm{k\ rms}\ \sin\theta)^{1.4} \tag{1}$$

$$\sigma^0_{VV} = 10^{-2.35}\left(\frac{\cos^{3}\theta}{\sin^3\theta}\right)10^{0.046\varepsilon_r\tan\theta}\lambda^{0.7}(\mathrm{k\ rms}\ \sin\theta)^{1.1}. \tag{2}$$

The algorithm is optimized for bare soils with $\mathrm{k} * \mathrm{rms} < 2.5$, soil moisture $< 0.35\ \mathrm{m}^3/\mathrm{m}^3$, and $\theta > 30°$ [2].

The more commonly used version of the Oh model (hereby referred to as the "2002" version [3]) relates the copolarized backscatter ratio p $(\sigma^0_{HH}/\sigma^0_{VV})$ and the cross-polarized ratio q $(\sigma^0_{\mathrm{HV}}/\sigma^0_{VV})$ to the volumetric soil moisture (mv) as a function

of incidence angle, wavenumber, surface rms, and correlation length (L) as

$$p = 1 - \left(\frac{\theta}{90^\circ}\right)^{0.35\ \mathrm{mv}^{-0.65}} e^{-0.4(\mathrm{k\ rms})^{1.4}} \tag{3}$$

$$q = 0.1\left(\frac{\mathrm{rms}}{\mathrm{L}} + \sin 1.3\theta\right)^{1.2}\left(1 - e^{-0.9(\mathrm{k\ rms})^{0.8}}\right) \tag{4}$$

$$\sigma^0_{HV} = 0.11\ \mathrm{mv}^{0.7}\cos^{2.2}\theta\left(1 - e^{-0.32(\mathrm{k\ rms})^{1.8}}\right). \tag{5}$$

The model is optimized within the soil moisture range of 0.09–0.31 $\mathrm{m}^3/\mathrm{m}^3$ and the roughness range of $0.1 < \mathrm{k} * \mathrm{rms} < 6$ [17]. Note that some of the fields listed in Table I are slightly outside such limits. However, in the case of semiempirical models, the validity domain is mostly associated to the range of the data used for the parameterization of the model and therefore is to be taken as the domain of "optimal performance" rather than "validity."

Also note that the cross-polarized scattering is assumed to be negligible in the backscatter direction by the Dubois model and IEM. For this reason and since the main objective of this paper is the comparison among the three models, the results presented are limited to the copolarized channels (HH and VV).

IV. Methods

SAR observation and ground data were averaged within each field listed in Table I on each observation date. Between 6 and 18 soil moisture measurements were averaged for each field. The field-average backscattering coefficients were calculated by averaging the linear (i.e., power units) single-look backscattering coefficients within the field boundaries, which were then converted to decibel units through logarithmic conversion. Field averaging of the geocoded single-look SAR data resulted in negligible speckle noise (the number of looks per field ranged approximately between 123 000 and 400 000) with respect to the PLIS system radiometric accuracy which is ± 0.8 dB [25]. Since the Dubois model and IEM are formulated directly as a function of the dielectric constant, the temperature corrected dielectric measurements provided by the dielectric probes were used as input for these two models. The dielectric constant was converted to soil moisture prior to input to the Oh model using soil-type-specific calibration functions developed for the study area [28].

Given the presence of periodic row structure at several of the fields analyzed (see Table I), the performance of the models was assessed using two different options concerning the surface roughness parameters used as input to the models. In the first case, it was assumed that the roughness scale relevant to the scattering is the fine scale (i.e., centimeters) associated with the soil clods and surface irregularities. In this case, the roughness parameters used as input were those measured in the direction parallel to the crop row direction. This was done under the assumption that the fine-scale roughness component is isotropic, which is well supported by photogrammetric studies of various surfaces [30]. In the second case, the coarser scale (i.e., tens of centimeters) roughness component associated with the periodic row structure was used as input for the model simulation. The parameters used in this case were those measured in the direction perpendicular to the crop rows. The two sets of input parameters are listed in Table I. It should be noticed that, for fields with no periodic row structure, no distinction was made between the fine- and coarse-scale roughness components. In such cases, the roughness parameters were taken as the average of those measured along the two cardinal directions.

The semiempirical calibration of the scattering models was applied in this study following the technique proposed in [8] and further developed in [9], [12], [22], and [23]. This was done in two stages: First, models were calibrated using calibration functions Lopt = f (rms) derived directly from the L-band data set used in this study. In the second stage, the robustness of the semiempirical calibration procedure was tested by applying calibration functions derived in previous studies [9], [22] to the present data set. The procedure adopted to calculate the calibration function Lopt = f (rms) for the present L-band data set followed that described in [9]. The known field-averaged soil moisture and surface rms values were used together with the observed field-averaged backscatter to calculate the population of fitting parameters Lopt which minimize the difference between the simulated and the observed backscatter. A "bootstrap" resampling technique was then adopted in order to assign a measure of accuracy to the parameters of the fitting function. To that end, 30 random resampling of the original data set were performed, and a function Lopt = f (rms) was fitted to each subsampled data set. Each of the 30 fitted functions was then applied to calibrate the IEM and the Oh model, and the "calibrated" backscatter error between the simulated and the observed backscatter was computed, together with the confidence intervals on such errors associated to the 30 "bootstrap" resampling. In the second stage, calibration functions derived in [9] and [22] were applied to the present data set. Several calibration functions were proposed in those studies. However, most of these were derived from C-band SAR data (ERS and RADARSAT). Given the strong dependence of the fitting parameter to sensor parameters (frequency, polarization, and incidence angle), ideally, only fitting parameters derived from L-band data sets having the same configuration of the present data sets should be applied. Although no calibration function was provided for L-band data in any previous study, individual values of the fitting parameter Lopt were provided in [9] for L-band acquisitions (Spaceborne Imaging Radar (Sir-C) sensor) in HH polarization at 44° to 57° incidence angles. For the purpose of cross-comparison with the present study, a calibration function was therefore derived from such data set. Despite the incidence angle being different from that of the present data set (25°–38°; see Table I), this calibration function was tested as it was the only other calibration function found in the literature for L-band data sets and as a comparison with the calibration function derived in this study for L-band. Moreover, given the availability in [22] of comprehensive calibration functions for C-band and HH and VV polarizations, parameterized as a function of the incidence angle between 20° and 50°, such functions were also tested in this study to assess the robustness of calibration functions derived from the same sensor configuration in terms of incidence angle and

TABLE II
IMPACT OF DIFFERENT ROUGHNESS PARAMETERIZATIONS ON THE BACKSCATTER SIMULATION ERROR USING THE IEM, DUBOIS, AND OH MODELS. FOR THE IEM, RESULTS ARE SHOWN USING BOTH AN EXPONENTIAL AND A GAUSSIAN ASSUMPTION CONCERNING THE SHAPE OF THE SURFACE ROUGHNESS ACF. FOR EACH POLARIZATION, THE MEAN ($\pm$ STANDARD DEVIATION σ) OF THE ERROR AND CORRELATION COEFFICIENT (r) BETWEEN SIMULATED AND OBSERVED BACKSCATTERS ARE SHOWN. ALL r VALUES ARE STATISTICALLY SIGNIFICANT ($p < 0.05$) EXCEPT THOSE INDICATED WITH ($*$)

Model	Roughness parameteriz. (Nr.pts)	HH-pol		VV-pol	
		Mean error (±st.dev.)	r	Mean error (±st.dev.)	r
IEM (exp.)	Fine (8)	1.9 (±2.1)	0.7	4.5 (±2.5)	0.8
	Coarse (8)	3.9 (±2.1)	0.9	5.0 (±1.9)	0.8
IEM (gaus.)	Fine (8)	4.6 (±1.9)	0.7	7.1 (±2.1)	0.8
	Coarse (8)	3.4 (±2.7)	-0.2(*)	4.1 (±3.6)	0.1(*)
Dubois	Fine (8)	1.8 (±2.0)	0.5	1.8 (±2.3)	0.7
	Coarse (8)	4.8 (±1.9)	0.9	4.2 (±2.2)	0.9
Oh (2002)	Fine (8)	-0.9 (±1.9)	0.5	-0.5 (±2.1)	0.6
	Coarse (8)	2.0 (±1.7)	0.8	2.0 (±2.0)	0.9

polarization, but different sensor frequency. A summary of the calibration functions used in this study can be found in the results section in Table IV.

The performance of the scattering models in simulating the observed backscatter is evaluated throughout the manuscript using the mean and standard deviation of the error between the simulated and the observed backscatter across all dates as well as the correlation coefficient between the simulated and the observed backscatter (r and level of significance p factor). The mean error is a measure of the overall offset between simulation and observed variables and can generally be attributed to systematic errors such as calibration offset or incorrect model parameterization. Conversely, the standard deviation of the error quantifies the random component of the error associated to nonsystematic factors (e.g., calibration and measurement noise, spatial heterogeneity of the input parameters).

V. RESULTS

A. Effect of Surface Roughness Parameterization

Before comparing the three scattering models, the impact of using the fine- or coarse-scale component of the surface roughness profiles was assessed for all models using fields #14, #79, and #24. These fields were selected as they presented an anisotropic and periodic tillage structure and had not been subjected to farming activities during the experiment (see Table I), ensuring that the analysis was unaffected by changes in surface roughness occurring between the dates of ground measurements and SAR acquisitions. Results are presented in Table II for each model and roughness parameterization (for the IEM, results are presented using both exponential and Gaussian approximations of the ACF). When using coarse-scale roughness, all models presented mean backscatter errors $> = 2$ dB, with errors as high as 5 dB (IEM in VV polarization). The most accurate among the three models was the Oh model, with mean errors equal to 2 dB for HH and VV polarizations (and error standard deviation of ± 1.7 and 2 dB, respectively). The use of the fine-scale roughness parameters resulted in a smaller offset between predicted and observed backscatters with respect to using the coarse-scale roughness, with a decrease of the mean error observed consistently across the three models and the two polarizations (except the IEM using the Gaussian ACF). The improvement was stronger for the IEM and the Dubois model (the mean error decreased respectively by up to 2 and 3 dB). When using fine-scale roughness, all models were accurate to within 2 dB (with a maximum error standard deviation of ± 2.1 dB), the only exception being the IEM (with exponential ACF) at VV polarization, which presented a mean error of 4.5 dB (± 2.5 dB), although this was improved with respect to using the coarse-scale roughness (5.0 dB $\pm$ 1.9 dB). The Oh model was the most accurate of the three models even when using fine-scale roughness, with mean errors of -0.9 dB (± 1.9 dB) and -0.5 dB (± 2.1 dB) for HH and VV polarizations, respectively, improved with respect to using the coarse-scale roughness of 1.1 and 1.5 dB, respectively.

It is worth noting that, despite the larger offset between predicted and observed backscatters, the use of coarse-scale roughness led to slightly higher correlation coefficients and smaller error standard deviation between the simulated and the observed backscatter (for IEM exponential, Dubois, and Oh model). This indicates the potential for a better fit of the models to observations if the significant biases were to be removed. Nevertheless, in the following analysis, the fine-scale roughness parameterization was adopted since it was the one providing, by far, the smaller offsets between the simulated and the observed backscatter (see Table II). The mean backscatter errors for individual fields (not shown in Table II) were higher for field #24 (mean errors between 4 and 7 dB for all models and polarizations) than for fields #14 and #79 (mean error < 5 dB). Note that field #24 was the only one with tillage rows oriented at $\sim 50^\circ$ from the PLIS radar bore sight as opposed to 90° for fields #14 and #79 (see Table I), indicating potential effects of the tillage row azimuthal direction on the model performance. The availability of only three fields with periodic structure does not allow a statistically significant analysis of this issue.

Results regarding the ACF shape effects on the IEM sowed that the exponential form led to a better match between predicted and observed backscatters when using fine-scale roughness for parameterization, with a decrease in the mean backscatter error of as much as 2 dB, with respect to using the Gaussian ACF. When using the coarse-scale roughness parameterization, although the exponential ACF resulted in slightly higher mean errors (by 0.5 and 0.9 dB for HH and VV polarizations, respectively), it also led to significantly smaller error standard deviation and better correlation between the predicted and the observed backscatter. Consequently, it seems that, regardless of the roughness parameterization, an exponential ACF is more appropriate (at least for the agricultural fields analysed), which is consistent with previous studies [9], [15], [17], [19]. The exponential ACF was therefore used in the following analysis.

TABLE III
COMPARISON BETWEEN THE BACKSCATTER SIMULATED BY THE IEM (WITH EXPONENTIAL ACF), DUBOIS, AND OH MODELS AND THAT MEASURED BY THE AIRBORNE SAR. FOR INDIVIDUAL FIELDS, ONLY THE MEAN ERROR BETWEEN SIMULATED AND OBSERVED BACKSCATTERS IS SHOWN. CUMULATED STATISTICS FOR FIELDS WITHOUT (∗) AND WITH (+) ACTIVITY OF FARMING MACHINERY ARE THEN SHOWN AS THE MEAN (AND STANDARD DEVIATION σ) OF THE ERROR AS WELL AS THE CORRELATION COEFFICIENT (r) BETWEEN SIMULATED AND OBSERVED BACKSCATTERS. THE BEST SIMULATIONS FOR EACH FIELD AND POLARIZATION ARE HIGHLIGHTED IN BOLD. ALL VALUES ARE IN DECIBELS. ALL R VALUES ARE STATISTICALLY SIGNIFICANT ($p < 0.05$) EXCEPT THOSE INDICATED BY (∗∗)

Field# (Nr.pts)	HH - pol			VV - pol		
	IEM	*Dubois*	*Oh (2002)*	*IEM*	*Dubois*	*Oh (2002)*
87*(3)	**-1.1**	-1.5	-5.0	2.3	**-1.3**	-3.7
48*(3)	2.7	2.7	**0.1**	5.0	2.3	**0.5**
49*(3)	4.9	5.6	**2.2**	6.5	4.8	**2.8**
50*(3)	0.7	**0.4**	-2.9	4.3	**1.0**	-1.1
14*(2)	**0.2**	-0.6	-3.6	3.8	**-0.4**	-3.0
79*(3)	**0.6**	1.2	-0.7	2.4	**0.7**	-1.0
24*(3)	4.3	3.9	**0.8**	7.1	4.3	**1.6**
All*(20)						
Mean (σ)	1.8 (2.3)	1.8 (2.5)	-1.2 (2.6)	4.5 (2.0)	1.7 (2.3)	-0.4 (2.4)
r	0.7	0.6	0.5	0.7	0.6	0.6
1+(3)	5.9	4.6	**2.1**	8.6	4.1	**2.2**
43+(3)	**0.6**	4.0	-1.7	3.8	4.4	**0.5**
51+(3)	7.2	7.5	**3.0**	9.8	7.1	**4.7**
70+(3)	5.6	5.8	**1.0**	7.9	4.6	**1.9**
All+(12)	4.8	5.5	**1.1**	7.5	5.0	**2.3**
Mean (σ)	4.8 (2.8)	5.5 (1.8)	1.1 (2.1)	7.5 (2.7)	5.0 (1.9)	2.3 (2.1)
r	0.04**	0.4**	0.1**	0.2**	0.2**	0.2**

B. Comparison Between Uncalibrated Models

The performances of the IEM (with exponential ACF), Dubois, and Oh models were then compared using data from all 11 fields listed in Table I, using the fine-scale roughness parameterization. The results are summarized in Table III. Overall, a reasonable agreement was observed between the modeled and the simulated backscatter for fields not farmed during the observation period. However, both the IEM and the Dubois model were found to overestimate the observed backscatter. The Dubois model equally overestimated the HH and the VV backscatter by approximately 1.8 dB (with an error standard deviation of ± 2.5 and 2.3 dB, respectively). The IEM performance was poorer for VV polarization where the observed backscatter was overestimated by as much as 4.5 dB (± 2 dB), while at HH polarization, the performance of the IEM was similar to that of Dubois (1.8-dB overestimation ± 2.3 dB). The Oh model exhibited the smallest mean backscatter error among the three models, with limited underestimation of the observed backscatter (mean errors of -1.2 ± 2.6 dB and -0.4 ± 2.4 dB for HH and VV, respectively). The skill of the Oh model with respect to the other two models was particularly significant in VV polarization (> 1.3-dB improvement in mean error), while at HH polarization, the improvement was only a fraction of a decibel (0.6 dB). It should be noted, although not shown in Table III, that all existing versions of the Oh model were tested in this study (the "1992" [17], "1994" [6], and "2004" [7] versions along with the "2002" [3] version). Since the 2002 version provided, by far, the smaller mean error between the observed and the simulated backscatter, it was the only one included in Table III. By comparison, the following mean errors were obtained in HH polarization (Oh 1992: -1.22 dB, Oh 1994: 2.1 dB, and Oh 2004: -1.6 dB) and VV polarization (Oh 1992: -0.4 dB, Oh 1994: 2.9 dB, and Oh 2004: -0.8 dB).

Larger discrepancies between simulated and observed backscatters were obtained for three of the four fields where farming activity was observed (except field #43 in HH polarization). Although this might be partially due to the fact that three of these fields (#43, #51, and #70) have incidence angles ($< 30°$) and soil moisture (> 0.35 m^3/m^3) slightly outside the validity domain for the Dubois and Oh models, the consistency of the backscatter error across three of the four fields for the IEM (which has larger validity domains than the Dubois and Oh models) and the loss of correlation between predicted and observed backscatters (r decreasing from 0.5–0.7 for fields without farming activities to less than 0.4 for fields with farming activities) indicate that this is likely the result of changes in surface roughness parameters having occurred between the date when the ground roughness measurements were taken and the SAR observations.

It is interesting to note that the IEM, despite having a larger mean error than the Oh model, exhibited the highest correlation coefficient (0.7) as well as the smallest error standard deviation among the three models (2.3 and 2 dB for HH and VV, respectively) for the nonfarmed fields. This suggested that the IEM had the potential to outperform the Oh model if the bias affecting it could be removed. This was further investigated in the next sections. It should also be noted that, in the following analysis, field #87 was removed from the analysis. This field presented a backscatter (between approximately -7 and -8 dB) much higher than those of all other bare surfaces with comparable roughness conditions (-10 to -17 dB), resulting in a underestimation of the observed backscatter by all models (see Table III). Visual inspection of optical aerial images and ground inspection revealed that these elevated backscatter values were associated with the presence of regular steep banks ($\sim$1 m high) bounding flooding rice bays within the paddock. Since such steep facets produce a strong coherent backscatter component which the models are not trained to simulated, the field was eliminated from subsequent analysis.

C. Dependence of the Uncalibrated Backscatter Error on Surface Conditions

The evaluation of scattering models conducted in previous studies has shown that a precise match between simulated and observed SAR backscatters is difficult to achieve. Even in the hypothetical absence of model error, errors deriving from surface roughness scale dependence and within-field variability or inaccuracy of the *in situ* measurements will introduce uncertainty. Similarly, scaling issues and within-field variability of soil moisture, as well as mismatches between the depths at

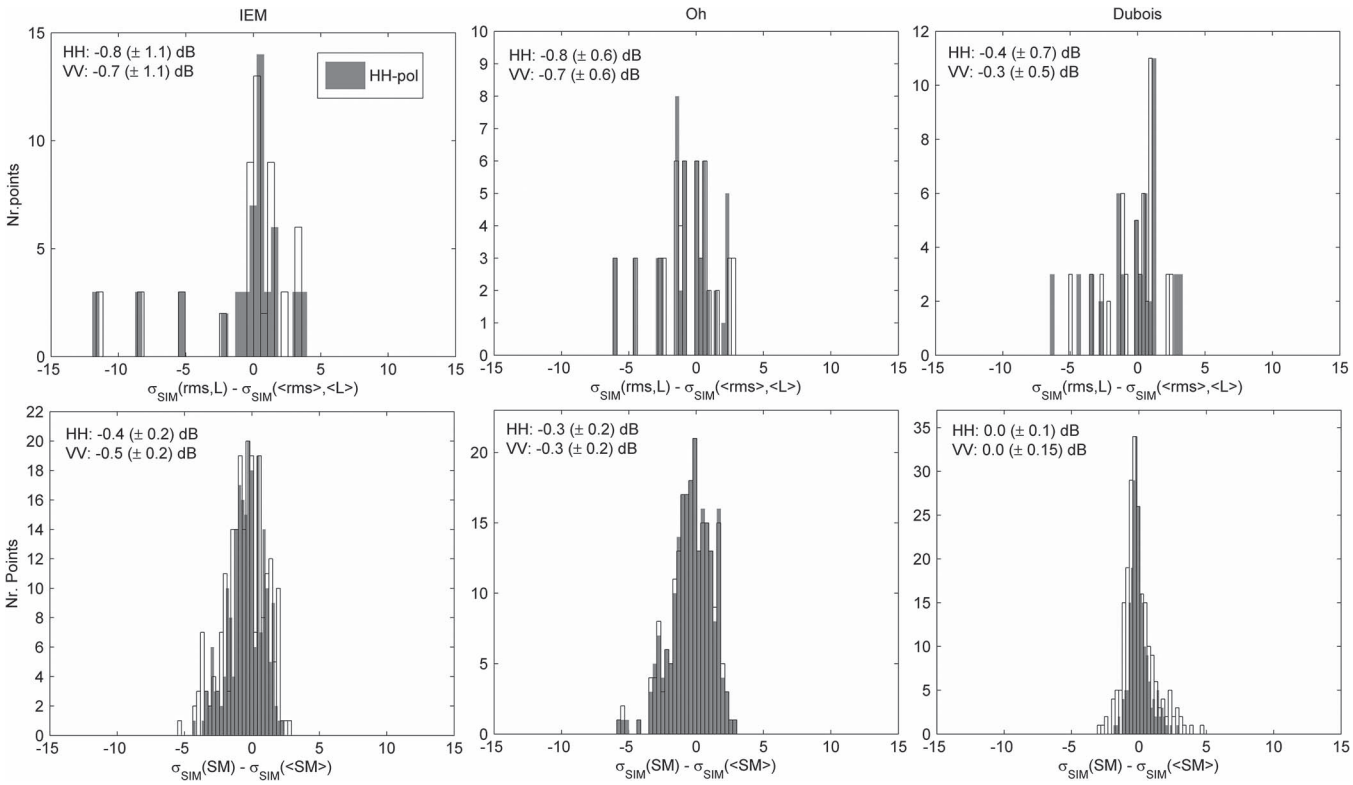

Fig. 1. Impact of within-field spatial variability of (top panels) surface roughness and (bottom panel) soil moisture on the performance of the IEM, Dubois, and Oh scattering models. Surface parameters considered are roughness root mean square (rms), correlation length (L), and soil moisture (SM). The histograms indicate differences between backscatter simulated (σSIM) using the point-scale measurements and the field-averaged values for each parameter ($\langle\langle\rangle\rangle$), with all other parameters set to the field-averaged value. Numbers indicate the mean difference for each model and polarization ($\pm 95\%$ confidence interval). The field-averaged conditions of the data presented range from 1.4–4.4 cm ($\langle\mathrm{rms}\rangle$), 8–26 cm ($\langle\mathrm{L}\rangle$), and 0.05–0.25 $\mathrm{m}^3/\mathrm{m}^3$ ($\langle\mathrm{SM}\rangle$).

which soil moisture is measured and the microwave effective penetration depth, will affect the accuracy of scattering models.

In order to analyze the potential impact of the within-field spatial variability of surface roughness and soil moisture on the results presented in Table III, the backscatters simulated by the three models when using field-averaged values of surface rms and correlation length ($\langle\mathrm{rms}\rangle$ and $\langle\mathrm{L}\rangle$) were compared with the backscatter simulated using the point-scale surface roughness measurements within each field when taken individually as input to the forward model. Similarly, the backscatter simulated using the field-averaged soil moisture ($\langle\mathrm{SM}\rangle$) was compared with that simulated using the individual soil moisture measurements within the field. The analysis was restricted to fields with at least three surface roughness measurements within the field boundaries, resulting in five fields with field-averaged conditions ranging from 1.4–4.4 cm ($\langle\mathrm{rms}\rangle$), 8–26 cm ($\langle\mathrm{L}\rangle$), and 0.05–0.25 $\mathrm{m}^3/\mathrm{m}^3$ ($\langle\mathrm{SM}\rangle$). Histograms of the resulting backscatter differences are displayed in Fig. 1, with mean differences and 95% confidence intervals also indicated for each model and polarization combination. Although a large error variability was observed (up to 10 dB), the difference between backscatter simulated using individual and field-averaged measurements was between -1.8 and 0.3 dB (within 95% confidence interval). The impact of the heterogeneity on surface roughness (rms and L) appeared stronger than that of soil moisture for all models, although this might be partially due to the fewest number of surface roughness measurements available, as indicated by the wider confidence intervals of the probability distribution for surface roughness heterogeneity (top panels in Fig. 1). Interestingly, the Dubois model was less impacted by the heterogeneity of both surface roughness and soil moisture than the IEM and the Oh model. When comparing mean differences in Fig. 1 with the mean simulation errors in Table III, it can be observed that only in the case of the Oh model was the combined uncertainty due to the heterogeneity of surface roughness and soil moisture roughly consistent (in magnitude and sign and taking into account the confidence intervals) to the mean backscatter error. This was not the case for the IEM and the Dubois model, particularly the IEM in VV polarization, indicating that additional sources of uncertainty are affecting the backscatter errors in Table III.

To understand whether the magnitude of the backscatter errors observed is associated to the magnitude of surface roughness (as opposed to its spatial variation), the field-averaged backscatter errors of Table III are plotted against the field-averaged surface rms and correlation length in Fig. 2. Given the limited number of data points, the determination coefficient adjusted for sample size (r2adj) was used in this case instead of the correlation coefficient. It should be noted that the relatively narrow soil moisture dynamic range experienced during the SMAPEx-3 experiment and the limited incidence angle range of the fields characterized by bare conditions did not allow the analysis of the dependence of the error on the field-average soil moisture and radar incidence angle. Despite the limited number of data points, the backscatter errors exhibited correlation with both the surface rms and correlation length. In HH polarization,

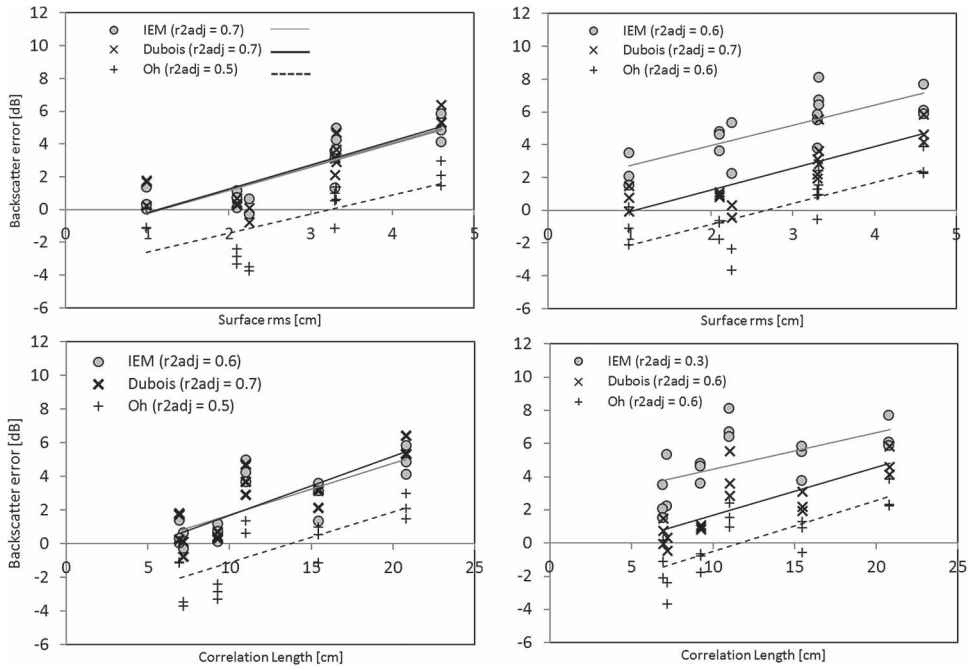

Fig. 2. Dependence of the error between model-simulated and SAR-observed backscatter on the (top row) field-averaged surface roughness root mean square and the (bottom row) correlation length for (left panels) HH and (right panels) VV polarizations. The determination coefficient (adjusted for the sample size) is shown in the legend for each case. All correlation coefficients are statistically significant $(p < 0.05)$. Only fields not subjected to farming activities during the observation period are included in this plot.

both the IEM and Dubois model errors were correlated with both roughness parameters ($\mathrm{r2adj} = 0.6$–0.7 with $p < 0.05$). Conversely, in VV polarization, only the Dubois model maintained a significant correlation with both roughness parameters ($\mathrm{r2adj} = 0.6$–0.7, with $p < 0.05$), while the IEM error was well correlated with the surface rms but poorly correlated with the correlation length (r2adj of 0.5 and 0.3, respectively, with $p < 0.05$). The backscatter error is seen to increase with increasing surface rms for the IEM and the Dubois model, with errors within ± 2 dB for surface rms up to 2.5 cm (except for IEM at VV polarization which exhibits a strong bias as commented earlier) and then increased up to $\sim$5–7 dB for surface rms values of $\sim$5 cm. The Oh model, despite having small mean errors as seen in the previous section, exhibited some correlation with the surface roughness parameters, particularly for VV polarization ($\mathrm{r2adj} = 0.6$, with $p < 0.05$). However, the Oh model provided a better match to the observed backscatter for rough surfaces $(\mathrm{rms} > 3\ \mathrm{cm})$.

Several previous studies have analyzed the reliability of surface roughness measurements carried out with manual profiles, indicating that the values obtained are highly variable and depend on the length of the profile used [18]. It has even been suggested that profiles as long as 40–200 times the correlation length might be needed to estimate surface rms and correlation length accurately [31]. Since both the IEM and the Oh model simulate the impact of the correlation length in their original formulation, the observed correlation of the model error to the ground-measured surface roughness parameters could reflect the inherent uncertainty in the measurement process for rough surfaces with larger correlation lengths, where the limited length of the profile used to characterize the surface roughness parameters becomes a limitation. In the next section, a semiempirical calibration of the correlation length is applied to investigate the potential improvement of the mismatch with SAR data observed.

D. Semiempirical Calibration of the Scattering Models

The semiempirical calibration procedure proposed in [8] and further developed in [9], [12], [22], [23] was applied in this study to assess the potential improvement of the mismatch between the observed and the simulated backscatter observed in previous sections. This was motivated first by the observed correlation between model errors and surfaces with elevated roughness (see Section V-C) and second by the fact that the IEM, despite presenting significant offset between the simulated and the observed backscatter, also exhibited the highest correlation coefficient and smaller error standard deviation among the three models (see Table III), indicating the potential for an improved backscatter prediction after the removal of such biases. The semiempirical calibration was applied in this study only to the IEM and the Oh model since, in its original formulation, the Dubois model was parameterized only as a function of soil moisture and surface rms, therefore not allowing for correlation length calibration.

Since the semiempirical calibration has not been applied before to L-band SAR data, it was necessary to first determine a suitable calibration function for each polarization. The fitting procedure was described in detail in the methodology (see Section IV), and the resulting calibration functions are shown in Fig. 3. It should be noted that calibration functions were calculated and applied individually to the IEM and the Oh model. This is because, as explained in [9] and [22], the fitting parameter Lopt is not a "corrected" correlation length, but rather, it

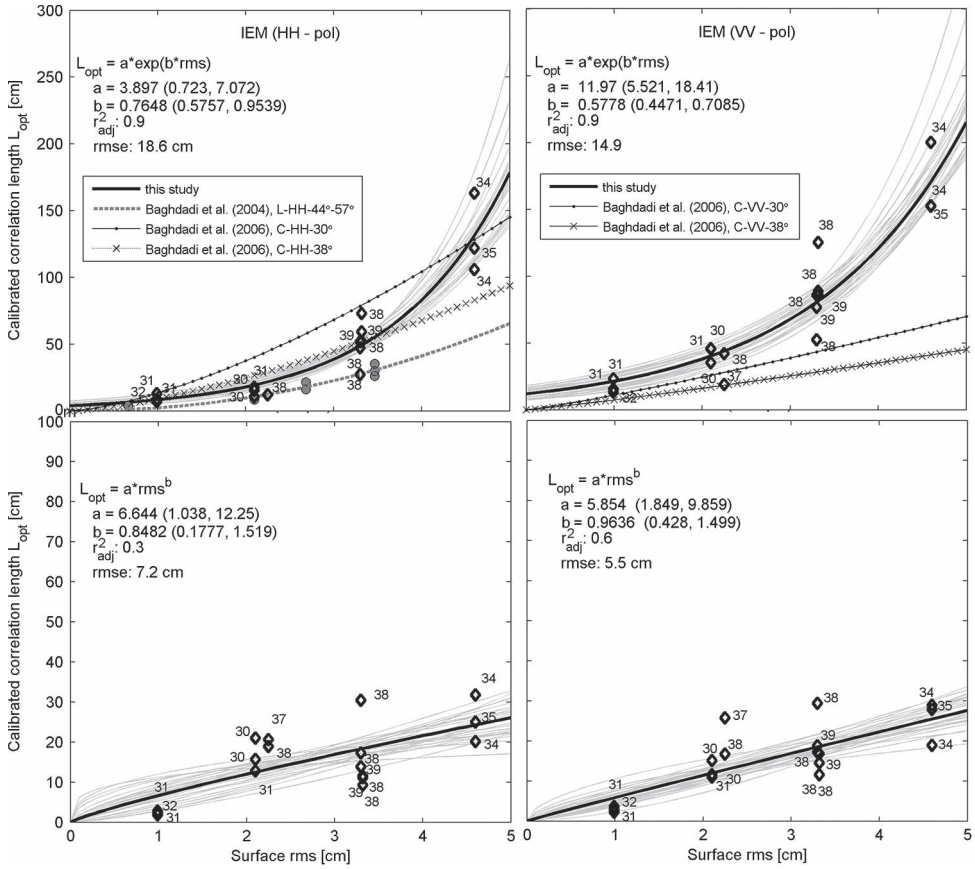

Fig. 3. Semiempirical calibration of the (top rows) IEM and (bottom row) Oh model. Diamond symbols indicate the population of fitting parameters L_{opt}, with numbers indicating the local incidence angle. The mean fitted function $L_{opt} = f(rms)$ (using all data) is shown as a thick black line, while thin gray lines correspond to the individual fittings of the 30 "bootstrap" resamples of the original data. The top-right text box in each panel provides the equation of the mean fitted function and its coefficients (with 95% confidence intervals corresponding to the "bootstrap" in brackets), as well as the determination coefficient (r2adj, adjusted for sample size) and root mean square error of the mean fitted function. Also shown are the calibration functions in [22] and [9] for various C-band and L-band configurations, (gray dots) the fitting parameter Lopt optimized in [9] for L-band SIR-C data, and the calibration function fitted in this study to the SIR-C data (L-HH-44-57).

is to be regarded as a calibration coefficient and is therefore specific to each model. With the present L-band data set, an exponential function was found to be the best fit for the fitting parameter Lopt of the IEM, whereas a power function was more suitable for the Oh model. However, it should be noted that the determination coefficients of the various functions explored (exponential, power, linear, and second polynomial) were very similar and all in excess of 0.8. Not surprisingly, given the small range of incidence angles of the available data (30°–38° excluding field #87; see Table I), Lopt was not seen to vary significantly with incidence angle. The fitted functions were quite similar for the two copolarized channels for the Oh model, while for the IEM, the calibrated Lopt for VV polarization was higher than that for HH polarization. In Table IV, the errors in simulated backscatter by the IEM and the Oh model after semiempirical calibration are compared with the performance of the uncalibrated models (from Table III less the eliminated field #87) for the case of fields without the activity of farming machinery. For the IEM, the calibration was able to correct the offsets between the observed and the simulated backscatter which affected the uncalibrated model, particularly bringing the mean backscatter error in VV polarization from 4.9 dB to −0.7 dB. Moreover, the correlation coefficients and error standard deviation were improved for both polarizations, indicating the ability of the calibration to compensate not only for systematic differences but also for random sources of error. For the Oh model, the calibration did not improve the model performance, with mean backscatter errors similar to the uncalibrated case and generally poorer correlation and larger error standard deviation than the IEM. After semiempirical calibration, the IEM outperformed the Oh model (both uncalibrated and calibrated) with respect to all the error metrics analyzed.

The gray curves shown in Fig. 3 represent the calibration functions fitted to the 30 subsampled data sets (using bootstrap). The narrow range of calibration curves indicates a good reliability of the exponential functions fitted, despite the limited data set. As a result of this, the confidence intervals on the error metrics shown in Table IV (which are derived from applying the 30 individual calibration functions), are fairly narrow, providing confidence that the improvement of the error metrics with respect to the uncalibrated models is statistically significant. Fig. 3 also displays the L-band and C-band calibration functions derived from [9] and [22], respectively, and used to independently evaluate the findings of this study. Since the C-band calibration functions were provided in [22] as a function of the incidence angle, in Fig. 3, the functions calculated for the minimum (30°) and the maximum (38°) incidence angle of the present data set are shown (calibration

TABLE IV
COMPARISON BETWEEN THE BACKSCATTER SIMULATED BY THE IEM AND OH MODEL AND THAT MEASURED BY THE AIRBORNE SAR BEFORE AND AFTER SEMIEMPIRICAL CALIBRATION. CALIBRATION RESULTS ARE PRESENTED USING DIFFERENT CALIBRATION EQUATIONS: (i) THOSE DEVELOPED IN THIS STUDY, (ii) THAT DERIVED IN THIS STUDY FROM L-BAND DATA AT HH POLARIZATION AND 44°–57° PRESENTED IN [9], AND (iii) THOSE PROPOSED IN [22] FOR C-BAND AND HH AND VV POLARIZATIONS AS A FUNCTION OF THE INCIDENCE ANGLE. THE MEAN AND STANDARD DEVIATION OF THE ERROR AND THE CORRELATION COEFFICIENT (r) ARE SHOWN FOR EACH CASE. FOR DATA CALIBRATED IN THIS STUDY, THE 95% CONFIDENCE INTERVALS ASSOCIATED TO 30 BOOTSTRAP SAMPLING CASES DURING CALIBRATION ARE REPORTED (±). ONLY FIELDS WITHOUT ACTIVITY OF FARMING MACHINERY WERE INCLUDED. FIELD #87 WAS EXCLUDED FROM THE ANALYSIS AS EXPLAINED IN THE TEXT. ALL VALUES ARE IN DECIBELS EXCEPT FOR THE CORRELATION COEFFICIENT r. ALL r VALUES ARE STATISTICALLY SIGNIFICANT ($p < 0.05$). VALUES OF THE COEFFICIENTS IN [22] ARE AS FOLLOWS: $\delta_{HH} = 4.026$, $\delta_{VV} = 3.289$, $\mu_{HH} = \mu_{VV} = -1.744$, $\eta_{HH} = \eta_{VV} = -0.0025$, $\varepsilon_{HH} = 1.551$, AND $\varepsilon_{VV} = 1.222$

	Calibration equation Lopt (band, polarisation, angle)	**HH - pol**			**VV - pol**		
		Mean	***St.dev.***	***r***	***Mean***	***St.dev.***	***r***
IEM							
Uncalibrated	*none*	2.3	2.0	0.7	4.9	1.9	0.8
Calibrated [This study]	*Lopt(L,HH,30-38°) = 3.897*exp(0.765*rms)* *Lopt(L,VV,30-38°) = 11.97*exp(0.578*rms)*	-0.3±0.1	1.1±0.02	0.8±0.01	-0.2±0.1	1.2±0.02	0.8±0.01
Calibrated using [9]	*Lopt(L,HH,44-57°) = 2.298*rms^(2.081)*	1.0	1.9	0.8	N/A	N/A	N/A
Calibrated using [22]	$L_{opt}(C) = \delta_{PP}(sin\theta)^{\mu_{PP}} * rms^{(\eta_{PP}\theta+\varepsilon_{PP})}$	-0.9	1.8	0.6	0.5	2.0	0.7
Oh (2002)							
Uncalibrated	*none*	-0.5	2.1	0.5	0.1	2.0	0.6
Calibrated [This study]	*Lopt(LHH, 30-38°) = 6.644*rms^(0.848)* *Lopt(L,VV, 30-38°)= 5.845*rms^(0.964)*	0.7 ±0.2	2.2±0.1	0.3±0.06	0.3±0.2	1.6±0.1	0.5±0.05

curves for the intervening range of 31°–37° will lie between these two reference curves). The function derived for L-band, HH polarization, and 44°–57° incidence angle (L-HH-44-57) was slightly lower than the fitting parameters calculated with the present data sets, which it followed reasonably well until the surface rms of ∼3.5 cm. For higher values of surface rms, the L-HH-44-57 underestimated the fitting parameters calibrated in this study. This is consistent with the decrease of fitting parameter with increasing incidence angle reported in [9] and [22]. Despite the difference in frequency, the C-band calibration functions matched reasonably well the fitting parameters calculated with the present data set for HH polarization, while at VV polarization, the L-band fitting parameters were significantly underestimated by the C-band calibration functions. This was a result of the fact that, at L-band, the fitting parameters for VV polarization were higher than those for HH polarization, whereas the opposite was found in [22] for C-band.

Results of the independent calibration of the IEM using the L-HH-44-57 calibration function and the C-band calibration functions are presented in Table IV. It should be noted that the L-HH-44-57 function was applied only to the HH data set as no calibration function was provided in [9] for VV polarization. Moreover, the C-band functions from [22] were applied by using the exact incidence angle available for each SAR observation (see Table IV). Notably, both functions led to an improvement of the performance of the IEM with respect to the uncalibrated case. In particular, the use of L-HH-44-57 decreased the mean backscatter error from 2.3 to 1 dB for HH polarization. The use of C-band calibration functions also significantly improved the performance of the IEM in both HH and VV polarizations, with a decrease in mean backscatter error from 2.3 to −0.9 dB (HH) and from 4.9 to 0.5 dB (VV). When compared to the performance of the Oh model, the IEM calibrated using the independent L- and C-band calibration functions outperformed the Oh model with higher correlation coefficients, smaller error standard deviation, and comparable mean errors.

VI. DISCUSSION

In this paper, a refined version of the Oh model [3] was tested and found to outperform both the IEM and the Dubois model in both HH and VV polarizations for a large range of surface roughness conditions (1.0–7.6 cm) and prior to any local recalibration. The skill of the Oh model with respect to the IEM and the Dubois model was particularly significant at VV polarization, for which the IEM overestimated the observed backscatter by up to 4.5 dB. Consistently with previous studies, the performances of the IEM and the Dubois model were found to be associated to surface roughness, with larger backscatter errors associated to rougher surface conditions (rms > 2.5 cm). Conversely, the Oh model was more robust across the range of roughness conditions analyzed. This indicate that, before any calibration was applied, the application of the Oh model would result in the smallest overall offset between simulated and observed backscatters among the three models. This is in contrast with previous studies which indicated that the Oh model has higher offsets than either the IEM or the Dubois model at L-band [14], [16]. Both studies nevertheless dealt with previous versions of the Oh model [17], which was, in this study, observed to be less accurate than the most recent version. However, despite the discrepancies on the offset magnitude for the various models, this study agrees with the analysis done at L-band in [14], [16], and [13] regarding the sign of these offsets: positive (overestimation) for the IEM and Dubois model and negative (underestimation) for the Oh model.

Results concerning the relative accuracy of the models, although performed in this study at L-band, are consistent with previous analysis undertaken at C-band [10], [16], [32], [33] in that the IEM predicted higher backscatters than the Oh model. However, the comparison with observed backscatters at C-band overall indicated better accuracy of the IEM over the Oh model at such frequency [16], [32], [33], particularly over smooth surfaces, in contrast with what was found in this study. Moreover, analysis of multipolarized C-band data in [10] indicated that the IEM correctly reflects the observed backscatter at VV polarization, but it has a tendency to overestimate the observed backscatter at HH polarization (2.9 dB). In this paper, the opposite was found for L-band, with the IEM exhibiting a stronger overestimation of the observed backscatter at VV polarization (4.5 dB) than at HH polarization (1.8 dB). Whether this is an effective deficiency of the IEM at L-band and VV polarization or rather a problem associated to instrumental error is an issue that requires confirmation using independent L-band data sets. In regard to the changes in model performance with increasing roughness, the results presented in this study for L-band agree well with observations done at C-band in that the IEM is more affected by increasing surface roughness, with a tendency to overestimation for rough surfaces and to underestimation for smooth surfaces, while the Oh model is more robust across the roughness range typical of agricultural areas [10], [16], [32], [33]. Therefore, our conclusions are that, at L-band, the Oh model is a better choice when no calibration is performed, as it provides a smaller mean error between the simulated and the observed backscatter and is also more robust with respect to increases in surface roughness.

It is also worth noting that discrepancies in results between this and the previous studies in regard to the performance of the various models might also depend on other factors, including the different surface conditions (soil moisture) and sensor characteristics (incidence angle). Consequently, the results presented are limited to relatively narrow range of incidence angles (24°–38°) and soil moisture (0.05–0.39 m^3/m^3). Variations in the quality of the absolute calibration between SAR data sets might also result in discrepancies when applying the same model. It should be noted that the calibration accuracy of the SAR data used in this study was ± 0.9 dB compared to ± 1–2 dB used in the previous studies [13], [14].

Despite the better accuracy of the uncalibrated Oh model in terms of mean error, it was noted that the uncalibrated IEM exhibited higher correlation coefficient and smaller error standard deviation. In the modeling of physical systems, such improved error metrics are generally symptomatic of a more physically sound response of the model to changing input parameters (in this case, soil moisture and surface roughness). The analysis of possible sources of uncertainty in the modeled backscatter, namely, the within-field variability of surface roughness and soil moisture, indicated that these are unlikely the cause of the offset observed for the uncalibrated IEM since they did not match, in either magnitude nor sign, the mismatch between simulated and observed backscatters. It was, in fact, observed that both the spatial variability in surface roughness and soil moisture would tend to result in an underestimation of the field-averaged backscatter, rather than an overestimation as generally observed in Table III.

The application of the semiempirical calibration of the correlation length performed in this study is the first independent verification of the procedure for L-band data at both HH and VV polarizations. As reported in previous studies [8], [9], [12], [22], [23], the fitting parameter Lopt was found to be linked to the surface rms. In this paper, an exponential function was found to be more suitable to model such dependence for the IEM instead of the power function proposed in [9] and [22]. After semiempirical calibration, the IEM outperformed the Oh model with respect to all the error metrics analyzed. It is important to notice that additional sources of uncertainty, not specifically analyzed here, could affect the comparison between the SAR-observed and the modeled backscatter. These include the measurement error of the dielectric probes used for soil monitoring as well as mismatch between the depth at which soil moisture is measured and the microwave effective penetration depth. The latter, in particular, might well result in a significant offset between the modeled and the observed backscatter. Therefore, one potential caveat of the analysis presented (already noted in [9]) is that the semiempirical calibration might just be absorbing whatever sources of uncertainty affect the mismatch between the observed and the simulated backscatter. However, the observed relationship between Lopt and surface rms, confirmed in this study, is a good indicator that the calibration parameter is likely to yield a physical meaning which can be exploited to derive a unique $\mathrm{Lopt} = \mathrm{f}\ (\mathrm{rms})$ law for each sensor configuration.

For the semiempirical calibration of the surface roughness correlation length to be valuable to global application, the fitting function should be robust, at least for a given sensor configuration (frequency, incidence angle, and polarization). Although no calibration functions where available in the literature for L-band data at the same incidence angle analyzed in this study, a good match between the simulated and the observed backscatter was achieved using calibration functions derived for different configurations, one for similar incidence angles but different SAR frequency (C-band versus L-band) and the other for the same frequency but different incidence angle range (30°–38° versus 44°–57°). Both calibration functions improved the performance of the uncalibrated IEM. Additionally, the calibrated IEM was more accurate than the Oh model (better error standard deviation and correlation coefficient and similar mean error).

Therefore, a significant outcome of this study is that it confirmed the robustness of the calibration procedures at L-band between different data sets. In particular, the differences between the calibration functions derived in this study and that derived from [9] for L-band and HH polarization are consistent with the decrease of fitting parameter Lopt with increasing incidence angle reported in [9] and [22]. The similarity between the L-band calibration functions derived in this study for HH polarization and the C-band functions proposed in [22] for the same incidence angles and polarization is also encouraging for the global application of the calibration procedure. Such similarity is consistent with the observation that changes of the calibration parameters between frequencies are of smaller

magnitude relatively to those associated with changes in incidence angle, for the range of configurations useful for remote sensing of soil moisture using SAR [9]. For example, as observed in [9] for a 4-cm surface rms, the C-band Lopt varied from 200 to 50 cm when going from a 21° incidence angle to ∼40°, but it only changed between 30 and 60 cm between C-band and L-band at 57°. It should be noted that the similarity between the L-band calibration functions derived in this study and the C-band functions proposed in [22] for the same incidence angles did not hold at VV polarization. However, this is a consequence of the low accuracy of the IEM which was affected by high overestimation errors at VV polarization in L-band (4.5-dB mean error; see Section V-B), while results reported in [22] for similar incidence angles showed much smaller biases in VV polarization at C-band (1.4 dB). Conversely, at HH polarization, the IEM performance was similar at L-band (1.8 dB) and C-band (2.4 dB), hence the similarity between the L- and C-band calibration functions for HH polarization. The result presented therefore supports the viability of a unified calibration function, provided that a relationship between Lopt and surface rms is available for the particular frequency, polarization, and incidence angle, which could be applied at global scale to improve the performance of the IEM without the need for local recalibration.

The Dubois model presented significant backscatter errors which could not be corrected through the same calibration procedure applied to the IEM and the Oh model. Since the Dubois model does not simulate the effect of the correlation length, the improvement of the model performance would require a modification of the original model parameters to fit the local conditions. This was not considered a valuable exercise toward the global application of SAR scattering models since it would certainly improve the performance of the model but most likely only for the local conditions. Conversely, the semiempirical calibration adopted for the IEM and the Oh model has the advantage of not modifying the model structure, but rather establishing an empirical relationship between roughness parameters (or at least their interdependence with respect to determining the surface scattering) which might turn out to be physically justifiable and therefore generally applicable.

The analysis on the impact of using different roughness parameters could also explain discrepancies between the observed accuracy of the various scattering models in different studies. Previous studies are not always clear on how the information from the ground profiles is used, but it is common practice in surface scattering studies to use the surface rms as calculated over the raw profile (i.e., no distinction of roughness scales). The results from this study indicate that, in the presence of anisotropic tillage structure, an improved backscatter prediction for the IEM and the Dubois model can be obtained when using the fine-scale roughness component associated with the soil clods and surface irregularities.

The comparison between the modeled and the observed backscatter was also observed to be strongly degraded on fields subjected to farming activities, due to changes in surface roughness occurring between the date when the ground roughness measurements were taken and the SAR observations. The information on farming dates received from the local farmers was not accurate enough (temporally) to allow improving the analysis for these fields. However, these results do highlight the strong impact of the assumption of temporal stability of surface roughness parameters which is frequently made in SAR-based soil moisture retrieval. The mean backscatter error over farmed fields was between 3 and 3.7 dB higher than that over non-farmed fields for the IEM and the Dubois model. The accuracy of the Oh model was less impacted by the farming activities in terms of mean error (the mean error was similar to that of the non-farmed fields), although these resulted in a positive bias (overestimation), particularly in VV polarization, and a significantly lower correlation coefficient.

VII. Conclusion

Three common surface scattering models were tested using airborne L-band multipolarized SAR data. The performance of the models was assessed both using surface roughness parameters measured by the ground profile as well as those derived from a semiempirical calibration procedure. The major findings of this study can be summarized as follows.

1) Comparison between uncalibrated models: Before calibration, the Oh model (2002 version) exhibited the best agreement between the simulated and the observed backscatter, with a mean error between the model-simulated and the SAR-observed backscatter of −1.2 dB (±2.6-dB error standard deviation) and −0.4 dB (±2.4 dB) for HH and VV polarizations, respectively. Larger backscatter errors were observed for the IEM, with mean errors of 1.8 dB (±2.3 dB) and 4.5 dB (±2 dB) for HH and VV, respectively, and for the Dubois model, with mean errors of 1.8 dB (±2.5 dB) and 1.7 dB (±2.3 dB), respectively. The skill of the Oh model with respect to the remaining models was particularly significant in VV polarization, where the IEM presented the highest errors. This observation warrants further analysis to establish whether this is an effective deficiency of the IEM at L-band and VV polarization or rather a problem associated to instrumental error.
2) Impact of the field-scale variability of soil moisture and roughness parameters: This was quantified to be between −1.8 and 0.3 dB, with the impact of the heterogeneity on surface roughness rms and correlation length being stronger than that of soil moisture for all models. However, such sources of errors did not fully explain model inaccuracies, particularly the large overestimation of the observed backscatter by the IEM at VV polarization.
3) The dependence of the uncalibrated model error on surface roughness conditions: The elevated backscatter errors for the IEM were found to be associated to rough surface conditions, with a mean error < 2 dB for smooth surface conditions $(\text{rms} < 2.5\ \text{cm})$ but increasing up to ∼5–7 dB for surface rms values of ∼5 cm. Poorer backscatter predictions were obtained when using the coarse-scale roughness component associated with the tillage structure, with an increase in backscatter mean error between 2–3 dB (for HH polarization) and 0.5–2.5 dB

(VV) with respect to the use of the fine-scale roughness component (i.e., associated with the soil clods and surface irregularities).

4) Model accuracy after semiempirical calibration: The application of an existing semiempirical calibration of the surface roughness correlation length led to a significant improvement in the performance of the IEM. After calibration, the IEM outperformed the Oh model, not only reducing the overall backscatter error to -0.3 dB (± 1.1 dB) and -0.2 dB (± 1.2 dB) for HH and VV polarizations, respectively, but also presenting significantly higher correlation between the simulated and the observed backscatter. The semiempirical fitting parameter was found to be related to the surface rms through an exponential function.
5) IEM semiempirical calibration for L-band SAR observations: Two exponential semiempirical calibration functions applicable to the IEM were fitted and tested. The calibration functions, applicable to L-band data in the 30–38° incidence angle range and HH and VV polarizations, respectively, complement similar calibration functions provided in [22] for C-band data. The analysis presented warrants further investigation using L-band observations at a wider range of incidence angles, in order to derive specific calibration functions for the IEM for a variety of L-band configurations (polarization and incidence angle) relevant to future L-band SAR missions with ScanSAR capabilities.
6) Robustness of the semiempirical calibration procedure: The fitting parameter derived in this study for L-band and HH polarization at 30–38° incidence angles was lower than that derived from an independent data set in [9] at the same configuration but higher incidence angles (44–57°), which is consistent with observations previously done at C-band on the decrease of the fitting parameter with increasing incidence angle. The calibration functions derived in [22] for the same incidence angles but different frequency (C-band) matched well the fitting parameters calculated in this study for HH polarization. Significant differences between the VV-polarized calibration curves at L- and C-bands were instead observed, as a consequence of the inaccuracies of the IEM in VV polarization at L-band. Nevertheless, the independent calibration functions in both frequencies were shown to improve the performance of the uncalibrated IEM at L-band, despite differences in frequency or incidence angles, suggesting that the calibration procedure is relatively robust and yields potential for future global application.

Acknowledgment

The authors would like to thank D. Gray, N. Stacey, A. Goh, and M. Williams for assisting with the polarimetric L-band imaging synthetic aperture radar calibration, Prof. J. T. Johnson from the Ohio State University for providing the code for the integral equation model, and F. Charbonneau and M. Trudel for providing the QuiP digital image processing package.

References

[1] A. K. Fung, Z. Li, and K. S. Chen, "Backscattering from a randomly rough dielectric surface," *IEEE Trans. Geosci. Remote Sens.*, vol. 30, no. 2, pp. 356–369, Mar. 1992.
[2] P. C. Dubois, J. v. Zyl, and T. Engman, "Measuring soil moisture with imaging radars," *IEEE Trans. Geosci. Remote Sens.*, vol. 33, no. 4, pp. 915–956, Jul. 1995.
[3] Y. Oh, "Semi-empirical model of the ensemble-averaged differential Mueller matrix for microwave backscattering from bare soil surfaces," *IEEE Trans. Geosci. Remote Sens.*, vol. 40, no. 6, pp. 1348–1355, Jun. 2002.
[4] T.-D. Wu and K.-S. Chen, "A reappraisal of the validity of the IEM model for backscattering from rough surfaces," *IEEE Trans. Geosci. Remote Sens.*, vol. 42, no. 4, pp. 743–753, Apr. 2004.
[5] T. D. Wu, K. S. Chen, J. Shi, H. W. Lee, and A. K. Fung, "A study of the AIEM model for bistatic scattering from randomly rough surfaces," *IEEE Trans. Geosci. Remote Sens.*, vol. 46, no. 9, pp. 2584–2598, Sep. 2008.
[6] Y. Oh, K. Sarabandi, and F. T. Ulaby, "An inversion algorithm for retrieving soil moisture and surface roughness from polarimetric radar observation," in *Proc. IGARSS*, Pasadena, USA, 1994, pp. 1582–1584.
[7] Y. Oh, "Quantitative retrieval of soil moisture content and surface roughness from multipolarized radar observations of bare soil surfaces," *IEEE Trans. Geosci. Remote Sens.*, vol. 42, no. 3, pp. 596–601, Mar. 2004.
[8] N. Baghdadi, C. King, A. Chanzy, and J. P. Wigneron, "An empirical calibration of the integral equation model based on SAR data, soil moisture and surface roughness measurement over bare soils," *Int. J. Remote Sens.*, vol. 23, no. 20, pp. 4325–4340, 2002.
[9] N. Baghdadi, I. Gherboudj, M. Zribi, M. Sahebi, C. King, and F. Bonn, "Semi-empirical calibration of the IEM backscattering model using radar images and moisture and roughness field measurements," *Int. J. Remote Sens.*, vol. 25, no. 18, pp. 3593–3623, Sep. 2004.
[10] N. Baghdadi and M. Zribi, "Evaluation of radar backscatter models IEM, OH and Dubois using experimental observations," *Int. J. Remote Sens.*, vol. 27, no. 18, pp. 3831–3852, Sep. 2006.
[11] A. Merzouki, H. McNairn, and A. Pacheco, "Evaluation of the Dubois, Oh, and IEM radar backscatter models over agricultural fields using C-band RADARSAT-2 SAR image data," *Can. J. Remote Sens.*, vol. 36, no. S2, pp. S274–S286, 2010.
[12] N. Baghdadi, J. Chaaya, and Z. M., "Semiempirical calibration of the integral equation model for SAR data in C-band and cross polarization using radar images and field measurements," *IEEE Geosci. Remote Sens. Lett.*, vol. 8, no. 1, pp. 14–18, Jan. 2011.
[13] F. Mattia, T. L. Toan, J.-C. Souyris, G. D. Carolis, N. Floury, F. Posa, and G. Pasquariello, "The effect of surface roughness on multifrequency polarimetric SAR data," *IEEE Trans. Geosci. Remote Sens.*, vol. 35, no. 4, pp. 954–966, Jul. 1997.
[14] J. R. Wang, A. Hsu, J. C. Shi, P. E. O'Neill, and E. T. Engman, "A comparison of soil moisture retrieval models using SIR-C measurements over Little Washita River Watershed," *Remote Sens. Environ.*, vol. 59, no. 2, pp. 308–320, Feb. 1997.
[15] J. Shi, J. Wang, A. Y. Hsu, P. E. O'Neill, and E. T. Engman, "Estimation of bare surface soil moisture and surface roughness parameter using L-band SAR image data," *IEEE Trans. Geosci. Remote Sens.*, vol. 35, no. 5, pp. 1254–1266, Sep. 1997.
[16] J. B. Boisvert, Q. H. J. Gwyn, A. Chanzy, D. J. Major, B. Brisco, and R. J. Brown, "Effect of surface soil moisture gradients on modelling radar backscattering from bare fields," *Int. J. Remote Sens.*, vol. 18, no. 1, pp. 153–170, Jan. 1997.
[17] Y. Oh, K. Sarabandi, and F. T. Ulaby, "An empirical model and an inversion technique for radar scattering from bare soil surfaces," *IEEE Trans. Geosci. Remote Sens.*, vol. 30, no. 2, pp. 370–381, Mar. 1992.
[18] N. E. Verhoest, H. Lievens, W. Wagner, J. Álvarez-Mozos, M. S. Moran, and F. Mattia, "On the Soil Roughness Parameterization Problem in Soil Moisture Retrieval of Bare Surfaces from Synthetic Aperture Radar Sensors," *Sensors*, vol. 8, no. 7, pp. 4213–4248, Jul. 2008.
[19] M. W. J. Davidson, T. Le Toan, F. Mattia, G. Satalino, T. Manninen, and M. Borgeaud, "On the characterization of agricultural soil roughness for radar remote sensing studies," *IEEE Trans. Geosci. Remote Sens.*, vol. 38, no. 2, pp. 630–640, Mar. 2000.
[20] N. Baghdadi, P. Paillou, M. Davidson, G. Grandjean, and P. Dubois, "Relationship between profile length and roughness parameters for natural surfaces," *Int. J. Remote Sens.*, vol. 21, no. 17, pp. 3375–3381, 2000.
[21] M. M. Rahman, M. S. Moran, D. P. Thoma, R. Bryant, E. E. Sano, C. D. Holifeld Collins, S. Skirvin, C. Kershner, and B. J. Orr, "A derivation of roughness correlation length for parameterizing radar backscatter models," *Int. J. Remote Sens.*, vol. 28, no. 18, pp. 3995–4012, Sep. 2007.

[22] N. Baghdadi, N. Holah, and Z. M., "Calibration of the integral equation model for SAR data in C-band and HH and VV polarizations," *Int. J. Remote Sens.*, vol. 27, no. 4, pp. 805–816, Feb. 2006.
[23] N. Baghdadi, E. Saba, M. Aubert, M. Zribi, and F. Baup, "Evaluation of radar backscattering models IEM, Oh, and Dubois for SAR data in X-band over bare soils," *IEEE Geosci. Remote Sens. Lett.*, vol. 8, no. 6, pp. 1160–1164, Nov. 2011.
[24] H. Lievens, N. E. C. Verhoest, E. De Keyser, H. Vernieuwe, P. Matgen, J. Álvarez-Mozos, and B. De Baets, "Effective roughness modelling as a tool for soil moisture retrieval from C- and L-band SAR," *Hydrol. Earth Syst. Sci.*, vol. 15, no. 1, pp. 151–162, Jan. 2011.
[25] R. Panciera, J. P. Walker, T. J. Jackson, D. Gray, M. Tanase, D. Ryu, A. Monerris, Y. Yardley, C. Rudiger, X. Wu, Y. Gao, and J. Hacker, "The Soil Moisture Active Passive Experiments (SMAPEx): Toward soil moisture retrieval from the SMAP mission," *IEEE Trans. Geosci. Remote Sens.*, vol. 52, no. 1, pp. 490–507, Jan. 2014.
[26] D. Gray, R. Yang, H. Yardley, J. Walker, B. Bates, R. Panciera, J. Hacker, A. McGrath, and N. Stacy, "PLIS: An airborne polarimetric L-band interferometric synthetic aperture radar," in *Proc. APSAR*, Seoul, Korea, Sep. 26–30, 2011, pp. 1–4.
[27] T. L. Ainsworth, L. Ferro-Famil, and J.-S. Lee, "Orientation angle preserving *a posteriori* polarimetric SAR calibration," *IEEE Trans. Geosci. Remote Sens.*, vol. 44, no. 4, pp. 994–1003, Apr. 2006.
[28] O. Merlin, J. Walker, R. Panciera, R. Young, J. Kalma, and E. Kim, "Soil moisture measurement in heterogeneous terrain," in *Proc. Int. Congr. MODSIM*, Christchurch, New Zealand, Dec. 2007, pp. 2604–2610.
[29] M. Trudel, F. Charbonneau, F. Avendano, and R. Leconte, "Quick Profiler (QuiP): A friendly tool to extract roughness statistical parameters using a needle profiler," *Can. J. Remote Sens.*, vol. 36, no. 4, pp. 391–396, Aug. 2010.
[30] X. Blaes and P. Defourny, "Characterizing bidimensional roughness of agricultural soil surfaces for SAR modeling," *IEEE Trans. Geosci. Remote Sens.*, vol. 46, no. 12, pp. 4050–4061, Dec. 2008.
[31] Y. K. Oh and Y. C., "Condition for precise measurement of soil surface roughness," *IEEE Trans. Geosci. Remote Sens.*, vol. 36, no. 2, pp. 691–695, Mar. 1998.
[32] M. Zribi, O. Taconet, S. LeHegaratMascle, D. VidalMadjar, C. Emblanch, C. Loumagne, and M. Normand, "Backscattering behavior and simulation comparison over bare soils using SIR-C/X-SAR and ERASME 1994 data over Orgeval," *Remote Sens. Environ.*, vol. 59, no. 2, pp. 256–266, Feb. 1997.
[33] L. Rakotoarivony, O. Taconet, D. Vidal-Madjar, and P. Bellemein, "Radar backscattering over agricultural bare soils," *J. Electromagn. Waves and Appl.*, vol. 10, no. 2, pp. 187–209, Jan. 1996.

Rocco Panciera (M'12) received the M.S. degree in environmental engineering from the University of Trento, Trento, Italy, in 2003 and the Ph.D. degree in environmental engineering from The University of Melbourne, Melbourne, Australia, in 2009.

He was then a Research Fellow with The University of Melbourne, Melbourne, within the Soil Moisture Active Passive project for algorithm development for National Areonautics and Space Administration (NASA) Soil Moisture Active Passive (SMAP) mission. In this role, he conducted two large-scale field experiments in southeastern Australia, including airborne active and passive microwave sensors. Since January 2011, he has held a postdoctoral position at the Cooperative Research Centre for Spatial Information, Melbourne, through the Super Science Fellowship from the Australian Research Council. In this role, he has been working on techniques to estimate fine-resolution soil moisture by the use of L-band and X-band synthetic aperture radar (SAR) measurements. His current field of interest is the retrieval of soil moisture from airborne and spaceborne SAR observations.

Mihai A. Tanase (M'12) received the engineering diploma in forestry from Stefan cel Mare University, Suceava, Romania, in 1999, the diploma in economy from the Bucharest Academy of Economic Studies, Bucharest, Romania, in 2004, the M.Sc. degree in environmental management from the International Centre for Advanced Mediterranean Agronomic Studies, Paris, France, in 2007, and the Ph.D. degree in geography from the University of Zaragoza, Zaragoza, Spain, in 2010.

Since 2011, he has held a postdoctoral position at The University of Melbourne, Carlton, Australia, through the Australian Research Council Super Science Fellowship program. He is a Principal Investigator for the European Space Agency (ESA), German Aerospace Agency (DLR), and Advanced Land Observation Satellite (ALOS)-2 projects and participated in the Kyoto and Carbon Initiative as a Coinvestigator. He is interested in the use of remote sensing for vegetation characterization. His current activity is focused on synthetic aperture radar (SAR), Interferometric Synthetic Aperture Radar, and Polarimetric Synthetic Aperture Radar data for fire severity estimation, fuel moisture content, vegetation recovery monitoring, and the retrieval of biogeophysical parameters of forests and agricultural crops.

Dr. Tanase was the recipient of the IEEE Geoscience and Remote Sensing Society (GRSS) International Geoscience and Remote Sensing Symposium (IGARSS) Interactive Prize Paper Award in 2010.

Kim Lowell received the B.Sc. degree (with honors) in forestry and the M.Sc. degree in forest biometrics from the University of Vermont, USA, in 1979 and 1981, respectively, and the Ph.D. degree in forest biometrics from Canterbury University, New Zealand, in 1984.

He has spent over 25 years working with spatial data to improve the management of landscapes and natural environments. He has a strong interest in quantifying and understanding spatial data quality to optimize geospatial research and development activities that improve environmental management and monitoring activities. He has worked in academia and government and has also collaborated with private industry on projects as diverse as carbon accounting, disaster management, and United Nations Educational, Scientific and Cultural Organization (UNESCO)-recognized areas. He is currently the Director of the Agriculture, Natural Resources, and Climate Change Program and a Professor at The University of Melbourne, Melbourne, Australia.

Jeffrey P. Walker (M'12) received the B.E. (Civil) and B.Surveying degrees with Hons 1 and University Medal and the Ph.D. degree in water resources engineering from the University of Newcastle, Australia, in 1995 and 1999, respectively.

His Ph.D. thesis was among the early pioneering research on the estimation of root-zone soil moisture from the assimilation of remotely sensed surface soil moisture observations. He then joined NASA Goddard Space Flight Center to implement his soil moisture work globally. In 2001, he moved to the Department of Civil and Environmental Engineering, The University of Melbourne, Melbourne, Australia, as Lecturer, where he continued his soil moisture work, including the development of the only Australian airborne capability for simulating new satellite missions for soil moisture. In 2010, he was appointed as Professor in the Department of Civil Engineering, Monash University, Melbourne, where he is continuing this research. He is contributing to soil moisture satellite missions at NASA, ESA, and Japanese Aerospace Exploration Agency, as a Science Definition Team member for the Soil Moisture Active Passive (SMAP) mission and Calibration/Validation Team member for the Soil Moisture and Ocean Salinity and Global Change Observation Mission-Water, respectively.